influence of breathing phases in intensity-modulated radiotherapy of lung tumours using four-dimensional CT," Br. J. Radiol. **83**, 252–256 (2010).
[27]K. Suga, Y. Kawakami, M. Zaki, T. Yamashita, K. Shumizu, and N. Matsunga, "Clinical utility of co-registered respiratory-gated $^{99m}$Tc-Technegas/MAA SPECT_CT images in the assessment of regional lung functional impairment in patients with lung cancer," Eur. J. Nucl. Med. Mol. Imaging **31**, 1280–90 (2004).
[28]M. Oliver, R. Staruch, A. Gladwish, J. Craig, J. Chen, and E. Wong, "Monte Carlo dose calculation of segmental IMRT delivery to a moving phantom using dynamic MLC and gating log files," Phys. Med. Biol. **53**, N187–N196 (2008).
[29]H. Wu, G. C. Sharp, Q. Zhao, H. Shirato, and S. B. Jiang, "Statistical analysis and correlation discovery of tumor respiratory motion," Phys. Med. Biol. **52**, 4761–4774 (2007).
[30]H. Shirato, S. Shimizu, K. Kitamura, T. Nishioka, K. Kagei, S. Hashimoto, H. Aoyama, T. Kunieda, N. Shinohara, H. Dosaka-Akita, and K. Miyasaka, "Four-dimensional treatment planning and fluoroscopic real-time tumour tracking radiotherapy," Int. J. Radiat. Oncol., Biol., Phys. **48**, 1187–1195 (2000).
[31]H. Wu, G. C. Sharp, B. Salzberg, D. Kaeli, H. Shirato, and S. B. Jiang, "A finite state model for respiratory motion analysis in image guided radiation therapy," Phys. Med. Biol. **49**, 5357–5372 (2004).

JJCO Japanese Journal of Clinical Oncology

*Jpn J Clin Oncol 2011;41(4)462–468*
*doi:10.1093/jjco/hyq231*
Advance Access Publication 22 December 2010

# Long-term Outcomes of Fractionated Stereotactic Radiotherapy for Intracranial Skull Base Benign Meningiomas in Single Institution

**Shunsuke Onodera[1,*], Hidefumi Aoyama[1], Norio Katoh[1], Hiroshi Taguchi[1], Kouichi Yasuda[1], Daisuke Yoshida[1], Ken Surtherland[2], Ryusuke Suzuki[2], Masayori Ishikawa[2], Bengua Gerard[2], Shunsuke Terasaka[3] and Hiroki Shirato[2]**

[1]Department of Radiation Medicine, Hokkaido University Graduate School of Medicine, [2]Department of Medical Physics, Hokkaido University Graduate School of Medicine and [3]Department of Neurosurgery, Hokkaido University Graduate School of Medicine, Sapporo, Japan

*For reprints and all correspondence: Shunsuke Onodera, Department of Radiation Medicine, Hokkaido University Graduate School of Medicine, North 15, West 7, Kita-ku, Sapporo 060-8638, Japan. E-mail: m950086@jasmine.ocn.ne.jp

Received May 6, 2010; accepted November 21, 2010

**Objective:** To investigate the outcome of linac-based fractionated stereotactic radiotherapy over the last 10 years for intracranial skull base benign meningiomas in patients who were inoperable, who had residual tumors with some components of high mitotic index after surgery and who experienced relapse of the tumor.

**Methods:** Twenty-seven patients with intracranial skull base benign meningiomas treated with fractionated stereotactic radiotherapy were retrospectively reviewed. Twenty-seven cases were diagnosed as benign meningiomas on pathological (17 cases) or radiological (10 cases) examination. The median follow-up time was 90 months after initial treatment and 63 months after fractionated stereotactic radiotherapy. The median biological equivalent dose calculated using an $\alpha/\beta$ ratio of 2.0 Gy was 82.0 Gy (range, 60–106 Gy).

**Results:** The 5-year overall survival was 95.7 (95% confidence interval: 87.3–100)% after initial treatment and 96.2 (88.8–100)% after fractionated stereotactic radiotherapy. The 5-year overall survival and local control rate of patients who received fractionated stereotactic radiotherapy alone were both 100%. The 5-year progression-free survival and local control rate after fractionated stereotactic radiotherapy were all 100% with a tumor volume of <9.1 cc and 68.2 (37.2–99.2) and 75.8 (45.2–100)% for the tumors 9.1 cc, respectively. The difference was significant in progression-free survival ($P = 0.022$) and local control rate ($P = 0.044$). The local control rate was significantly worse in patients who received fractionated stereotactic radiotherapy for relapsed tumors ($P = 0.01$). No late radiation damage was observed in the follow-up period.

**Conclusions:** The long-term outcome suggests that fractionated stereotactic radiotherapy is a safe and effective treatment for intracranial skull base benign meningioma, especially for those who have tumors <9.1 cc or would receive fractionated stereotactic radiotherapy with or without surgery as the initial treatment.

*Key words: radiation therapy – meningioma – stereotactic – skull base – fractionation*

## INTRODUCTION

Radiotherapy is increasingly being used for the treatment of meningiomas after incomplete resection, after recurrence and when tumor histology is atypical or malignant (1,2). When meningiomas are located in the intracranial skull base region, tumor excision is frequently incomplete and even biopsy can be hazardous (1). Therefore, it is a matter of

debate whether the use of radiotherapy should be used when the residual tumor is still small as the primary treatment or should be reserved as a potential salvage treatment for the residual tumor enlarged (3).

Stereotactic radiosurgery (SRS) has been proven useful for reducing unnecessary irradiation to the normal tissue surrounding meningiomas and provides an excellent local control rate (LCR) for small to mid-size skull base meningiomas (3,4). Three-dimensional conformal radiotherapy (3D-CRT) and fractionated stereotactic radiotherapy (FSRT) are expected to be useful for further reducing the possibility of late adverse reactions, even for relatively large tumors (5,6). Although there were several precise reports from a few institutions about the long-term outcome after FSRT (5–8), we are still short of knowledge about the treatment results of FSRT with the median follow-up longer than 60 months for intracranial meningioma.

We began using FSRT 15 years ago for patients with intracranial skull base meningiomas, principally for patients who were inoperable, who had residual tumors with some components of high mitotic index or high MIB-1 index, who experienced relapse of the tumor. In this study, we retrospectively reviewed our long-term results for FSRT of intracranial skull base benign meningiomas in order to investigate the usefulness and prognostic factors of this treatment.

## PATIENTS AND METHODS

### Patients

The outcome of 27 patients with intracranial skull base benign meningiomas treated with FSRT at Hokkaido University Hospital between May 1994 and February 2009 was retrospectively reviewed. Our treatment policy was to apply FSRT principally for those patients with intracranial skull base meningiomas who were inoperable, who had residual tumors or who experienced relapse of the tumor.

The patients' characteristics are summarized in Table 1, which were classified by the treatment category. In our cases, diagnosis was based on pathological examinations in 17 patients and radiological characteristics in 10 patients. The tumor was located at lateral structures in 17 (anterior fossa in 2, middle-lateral sphenoid wing in 8 and cerebellopontine angle and posterior fossa in 7 patients) and at central structures in 10 patients (cavernous sinus and tuberculum sellae in all 10 patients). The median tumor volume was 9.1 (range: 1.1–86.1) cc in all benign meningiomas. The median tumor volume in the initial treatment group was smaller than that in the salvage treatment group (6.3 vs. 12.3 cc), but there was no significant difference statistically ($P = 0.139$; Mann–Whitney test).

In this study, 11 patients were treated with FSRT alone as the initial treatment: 1 after biopsy (Simpson's grade V) and 10 after radiological diagnosis. Radiotherapy was used as a part of the initial treatment after incomplete excision in 4 patients and as a salvage treatment for tumor recurrence after surgery in 12 patients. The number of surgical procedures before FSRT was 1, 2 and 3 in 10, 5 and 1 patients, respectively. Patients who received open biopsy or surgery were classified according to Simpson's grade (9). Simpson's grade II (complete removal and coagulation of dual attachment) and IV (subtotal resection) surgery before radiotherapy was performed in 1 and 15 patients, respectively. Only one patient received biopsy (Simpson's grade V).

**Table 1.** Patients' characteristics

| Factors | Initial treatment group | Salvage treatment group | Total |
|---|---|---|---|
| Total | 15 | 12 | 27 |
| Diagnosis | | | |
| Pathological diagnosis | 5 | 12 | 17 |
| Radiological diagnosis | 10 | 0 | 10 |
| Sex | | | |
| Male | 1 | 6 | 7 |
| Female | 14 | 6 | 20 |
| Age | | | |
| Mean (range) | 60.3 (18–78) | 45.5 (14–72) | 53.7 (14–78) |
| Tumor cite | | | |
| Lateral | 11 | 6 | 17 |
| Central | 4 | 6 | 10 |
| Gross tumor volume | | | |
| Median (range) (cc) | 6.3 (1.1–58.9) | 12.3 (2.5–86.1) | 9.1 (1.1–86.1) |
| Simpson's grade | | | |
| I | 0 | 0 | 0 |
| II | 0 | 1 | 1 |
| III | 0 | 0 | 0 |
| IV | 4 | 11 | 15 |
| V | 1 | 0 | 1 |
| Radiotherapy alone | 10 | 0 | 10 |

### Radiation Therapy Method

The gross tumor volume (GTV) was taken as the gross tumor shown on computed tomography (CT) with or without magnetic resonance imaging (MRI). The clinical target volume (CTV) was equal to the GTV, post-operative tumor bed or both in this study. The planning target volume (PTV) was 2–3 mm geometric expansion of the CTV. In delineating GTV, MRI co-registered with CT was used in 18 recent patients, and only the CT information was used for the remaining 9 patients.

Treatment planning systems were Focus or Xio (CMS Japan, Japan). A dose calculation algorithm used for the skull base meningiomas was the Clarkson method or the

convolution method. Stereotactic radiotherapy was carried out by using a 6 or 10 MV linear accelerator (LINAC) (2100C: Varian, Palo Alto, CA, USA; EXL15DP: Mitsubishi, Japan) with an in-house developed LINAC-based SRT system. Three-dimensional non-coplanar, single isocenter and the technique using multileaf collimator (MLC) were used. Three to eight static non-coplanar ports with the conformal fields were used in general. The width of these leafs was 5–10 mm at the isocenter. The dose was prescribed at the isocenter and defined as 100% in the dose distribution profile. MLCs were opened to cover PTV by a 90–95% isodose shell. The maximum dose point was always situated near the isocenter with the dose <110% (Fig. 1).

Patients were fixed by using a thermo-plastic mask and a custom-made head rest system. The dose to the optic chiasm was limited to ≤46 Gy. The total dose was 48–54 Gy in 26 cases and 32 Gy in 1 case using 2.0 Gy as the daily dose. When these radiation schedules were converted into the biological equivalent dose (BED) using an $\alpha/\beta$ ratio of 2.0 Gy, the median BED dose was 82.0 Gy (range: 52–90 Gy).

### Follow-up and Statistical Analyses

The median follow-up time was 90 months (range: 21–209 months) after initial treatment, surgery or FSRT. The median follow-up time was 63 months (range: 19–154 months) after FSRT. More than 70% of patients were followed longer than 36 months after FSRT. Patients were periodically monitored by physical as well as radiographic examination in Hokkaido University Hospital and related hospitals. Local tumor progression (PD) was scored when the maximum diameter of the tumor increased 2 mm or more and partial reaction was scored when the diameter decreased 2 mm or more. The LCR was defined as no change or decrease of the tumor volume in the anatomical region consistent with the PTV of the treatment planning image. When more than 80% of the relapsed tumor volume was outside of the PTV, the recurrence was defined as out of field (10). In-field (>95% of the relapsed tumor volume in the PTV), marginal (20–95% of the relapsed tumor volume in the PTV), and out-of-field (less than 20% of the relapsed tumor volume in the PTV) recurrence were defined in this study.

Statistical analyses were conducted by using commercially available software (SPSS v18; IBM Inc., Chicago, IL). The overall survival (OS) and LCR were calculated from the date of the initiation of radiotherapy using the Kaplan–Meier method, and statistical evaluations were carried out by the log-rank test.

## RESULTS

The OS, progression-free survival (PFS) and LCR at 5 years after initial treatment were 95.7 [95% confidence interval (CI): 87.3–100], 91.6 (80.4–100) and 95.5 (86.9–100)%.

The OS, PFS and LCR at 5 years after FSRT were 96.2 (88.8–100), 84.6 (67.7–100) and 88.6 (72.9–100)%.

Partial response was achieved in two benign patients, and the other patients with local control experienced no change of tumor volume. Three (11%) patients experienced in-field recurrence. These tumors had received Simpson's grade IV surgical resection. One patient had progression disease out of irradiation field. The recurrent cases were observed at the posterior fossa (at 55 and 81 months) in two patients, and at the cavernous sinus and tuberculum (at 19 and at 27 months) in two patients. These four recurrent cases are summarized in Table 2. No marginal recurrence was observed.

Univariate analyses were performed on OS, PFS and LCR after FSRT for patients with benign meningioma (Table 3). The female patients had significantly better PFS ($P = 0.009$) and LCR ($P = 0.04$) than the male patients. The 5-year OS, PFS and LCR after FSRT were all 100% for the benign meningiomas with a tumor volume of <9.1 cc and these parameters were 91.7 (76.0–100), 68.2 (37.2–99.2) and 75.8 (45.2–100)% for the tumors >9.1 cc, respectively. The difference was significant in PFS ($P = 0.022$) and LCR ($P = 0.044$) (Fig. 2).

In this study, the 11 patients who received FSRT alone had 100% OS, 88.9% PFS and 100% LCR at 5 years, respectively. The OS, PFS and LCR of patients who received FSRT with or without surgery as the initial treatment ($n = 15$) were 100, 91.7 and 100%, whereas those of patients who received FSRT for relapse ($n = 12$) were 90.9, 68.2 and 68.2%, respectively. The LCR was significantly worse in patients who received FSRT for a relapsed tumor ($P = 0.01$). A higher biological radiation dose, BED, was paradoxically associated with a lower PFS and LCR. The median tumor volume was larger (11.0 vs. 6.7 cc) and the ratio of patients with relapsed tumor was higher (7/11 vs. 5/16) in the higher

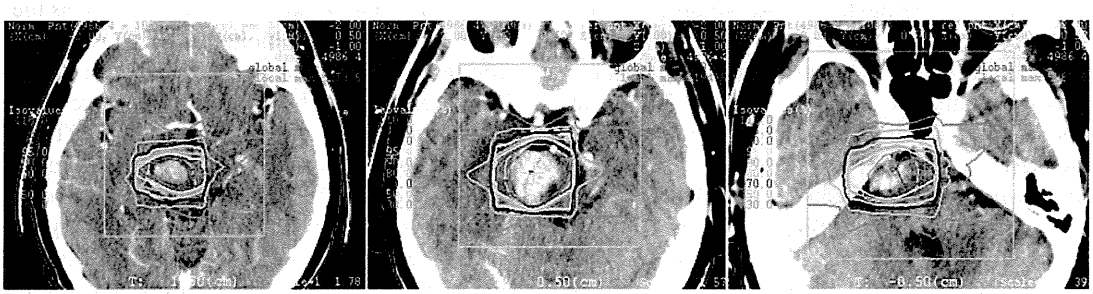

**Figure 1.** Dose distribution of FSRT for an intracranial benign meningioma. FSRT, fractionated stereotactic radiotherapy.

**Table 2.** The characteristics of patients with skull base benign meningioma who experienced tumor recurrence after FSRT either in-field or out-of-field

| No. | Age | Sex | Primary site | Gross tumor volume (cc) | Simpson's grade | FSRT for relapsed tumor | Dose/fraction (Gy/fraction) | Local control | Recurrent site | Relapse (months) | Survival times | Final status |
|---|---|---|---|---|---|---|---|---|---|---|---|---|
| 1 | 78 | M | Cavernous sinus | 58.9 | Grade V | No | 54 Gy/27fr | NC | Out-of-field | 27 | 27 | Alive |
| 2 | 35 | M | Cerebellopontine angle | 9.75 | Grade IV | Yes | 54 Gy/27fr | PD | In-field | 81 | 81 | Alive |
| 3 | 51 | M | Cerebellopontine angle | 13.9 | Grade IV | Yes | 44 Gy/22fr + 10 Gy/4fr | PD | In-field | 55 | 55 | Alive |
| 4 | 58 | F | Tuberculum sellae | 24.9 | Grade IV | Yes | 54 Gy/27fr | PD | In-field | 19 | 20 | Death |

FSRT, fractionated stereotactic radiotherapy; NC, no change; PD, progression of disease.

**Table 3.** The univariate analysis of prognostic factors after FSRT in patients with skull base benign meningiomas

| Factor | 5-year OS (95% CI) | *P* value | 5-year PFS (95% CI) | *P* value | 5-year LCR (95% CI) | *P* value |
|---|---|---|---|---|---|---|
| Age | | | | | | |
| >60 ($n = 11$) | 100 | 0.429 | 87.5 (64.6–100) | 0.703 | 100 | 0.219 |
| ≤60 ($n = 16$) | 93.8 (81.8–100) | | 82.0 (58.1–100) | | 82.0 (58.1–100) | |
| Gender | | | | | | |
| Female ($n = 20$) | 95.0 (85.4–100) | 0.584 | 94.7 (84.7–100) | 0.009 | 94.7 (84.7–100) | 0.04 |
| Male ($n = 7$) | 100 | | 55.6 (7.0–100) | | 66.7 (13.4–100) | |
| Gross tumor volume | | | | | | |
| <9.1 cc ($n = 14$) | 100 | 0.28 | 100 | 0.022 | 100 | 0.044 |
| ≥9.1 cc ($n = 13$) | 91.7 (76.0–100) | | 68.2 (37.2–99.2) | | 75.8 (45.2–100) | |
| Planning method | | | | | | |
| With MRI fusion ($n = 18$) | 94.1(82.9–100) | 0.467 | 86.5 (69.1–100) | 0.229 | 93.8 (81.8–100) | 0.473 |
| Without MRI fusion ($n = 9$) | 100 | | 87.5 (64.6–100) | | 87.5 (64.6–100) | |
| Treatment for recurrence | | | | | | |
| No ($n = 15$) | 100 | 0.243 | 91.7 (76.0–100) | 0.102 | 100 | 0.013 |
| Yes ($n = 12$) | 90.9 (73.8–100) | | 68.2 (27.6–100) | | 68.2 (27.6–100) | |
| Biological effective dose (Gy) ($\alpha/\beta = 2$) | | | | | | |
| ≥85 ($n = 11$) | 90.9 (73.8–100) | 0.243 | 60.6 (21.8–99.4) | 0.006 | 68.2 (27.6–100) | 0.013 |
| <85 ($n = 16$) | 100 | | 100 | | 100 | |

OS, overall survival; CI, confidence interval; PFS, progression-free survival; LCR, local control rate; MRI, magnetic resonance imaging.

dose group than the lower dose group, although the difference did not reach the level of statistical significance.

No adverse event was observed in the follow-up period. No optical injury, temporal lobe injury or hydrocephalus, or symptoms related to radiotherapy were observed.

## DISCUSSION

The median dose used in the present study is 48–54 Gy with daily dose of 2.0 Gy. It is lower than the dose used in the Heiderberg study (5,7), in which the mean radiation dose was 56.8 Gy (±4.4 Gy), and higher than the dose used in the French study (8), in which 45 Gy with daily dose of 1.8 Gy was used. Since a dose–response curve for normal tissues and tumor changes rapidly at the dose range from 40 to 60 Gy with 1.8–2 Gy fractional dose, our results add new biological data for the meningioma and surrounding normal tissue with the long follow-up.

We found that the OS and LCR were 100% at 5 years after FSRT alone for patients with benign skull base meningioma who received FSRT as the initial treatment. This is consistent with a recent article by Korah et al. (6) in which the 8-year LCR was 94% after radiotherapy alone for

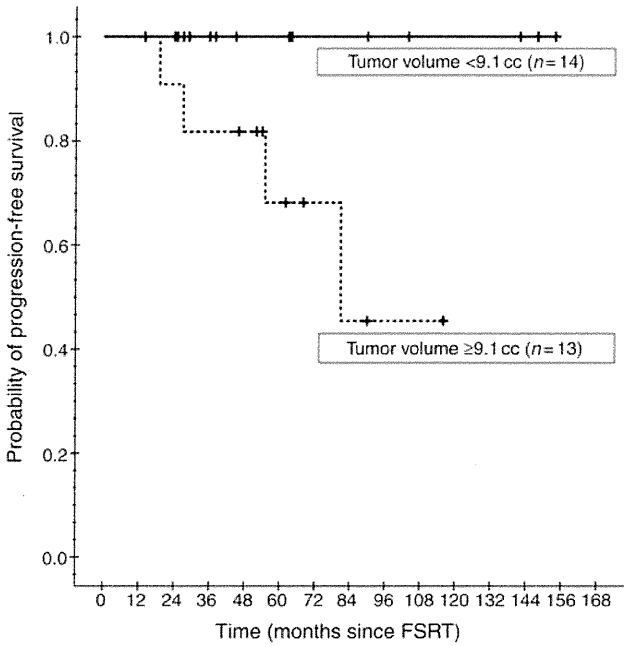


**Figure 2.** Progression-free survival curves according to the tumor volume. The patients were divided at a median volume of 9.1 cc.

42 patients. Lee et al. (10) also reported a 96.9% LCR at 5 years after SRS alone for 83 patients with cavernous sinus meningiomas. Other series have also suggested a high LCR after radiotherapy alone for benign meningiomas (4,5,11).

After incomplete surgical resection of Simpson's grade III or IV, the recurrence rate of meningiomas is high without radiotherapy (12,13). The recurrence rates for skull base meningioma are especially high, because total resection is much more difficult at this site than at other sites (12,14,15). Adjuvant FSRT immediately after subtotal resection has been suggested to reduce the recurrence rate without lowering the complication rate compared with previous radiotherapy (1,16,17). Previous reports have suggested that radiotherapy for recurrent meningioma is more difficult than radiotherapy used as the initial treatment (14,18). Condra et al. (1)reported that the cause-specific survival was better in patients who received radiotherapy immediately after subtotal resection than those who did not receive radiotherapy. Milker-Zabel et al. (5) also found that patients treated for recurrent meningioma showed a trend toward decreased PFS compared with patients treated with primary therapy, after biopsy or after subtotal resection ($P < 0.06$) in 179 patients with benign or atypical meningiomas.

Our results also suggested that better LCR were obtained for patients who received FSRT with or without surgery as the initial treatment than for those who received FSRT for relapsed tumors. However, the number of patients who were surgically treated and had residual tumor in our institution is uncertain. A small amount of residual benign meningioma after total or subtotal removal often does not enlarge or become symptomatic. Therefore, there is a possible bias that delayed irradiation was given for a poor prognosis group with a tendency of enlargement and irradiation was not required at all for the majority of patients in a good prognosis group. Precise selection criteria for the early irradiation after surgery are warranted to reduce the unnecessary irradiation for the good prognosis group.

The poorer outcome for recurrent meningioma is likely due to the progressive nature of some meningiomas or a mixed component of atypical meningioma (4,19,20). Meningiomas have been reported to obtain radioresistance or a component of malignant transformation as a natural course of the disease (20–23).

Considering that relapsed meningiomas often contain a progressive component, the treatment policy of applying radiotherapy only in the case of relapsed tumors causes a selection bias in the treatment outcome. The progressive nature of some meningiomas may also result in a leading bias with the treatment policy. Our study showed that the 5-year OS was 96.3% after any initial treatment and 88.2% after FSRT for the same patients' group. We summarized the previous studies of SRS and FSRT in Table 4 and found that our results contained the largest proportion of the relapsed tumors in these series. The tendency for the outcome to be better in the series with a lower proportion of relapsed tumors was not negligible. The lack of these biases may partly explain the excellent results in the group that received radiotherapy alone. The present study suggested that the selection bias and leading bias must be held in mind when we compare the treatment results of radiotherapy among different institutions or compare it with surgical series.

This study showed that the tumor volume was a significant prognostic factor as reported previously (5,22). We summarized the previous studies of SRS and FSRT which discriminated the tumor volume of benign tumors from atypical and malignant meningiomas (Table 4). The median tumor volume was 10 cc less in the majority of studies (4,10,11,24–29). The 5-year PFS and LCR values were more than 90% in these series. This study showed that our results of FSRT for tumors <9.1 cc (median) were as good as those in the previous studies. However, for the total patient group, including patients with larger tumors, the 5-year PFD and LCR were 84.6 and 88.6%, respectively. This finding is consistent with the results of Subach et al., who reported a mean tumor volume of 13.7 cc and a reduction of 5-year LCR to 86% (24).

Conventional 3D-CRT was reported to achieve excellent results in 1980s–early 1990s when CT and MRI images had 5 mm slice thickness and very precise fixation did not make sense. However, in the late 1990s, treatment planning using images with 1–2 mm thickness began to require precise fixation of the skull. Although there is no randomized studies to compare 3D-CRT and FSRT, FSRT can reduce the dose to the critical part of brain tissue with higher certainty than conventional 3D-CRT in the era of 1–2 mm slice thickness of the medical images. There are two recent reviews comparing different radiotherapy techniques such as 3D-CRT, SRS

**Table 4.** Previous studies of stereotactic radiosurgery and fractionated stereotactic radiotherapy for skull base benign meningioma in which the median or mean tumor volume was described for benign tumors

| Institution | SRS or FSRT | No. of patients | Tumor volume median (range) (cc) | Recurrent cases (%) | Follow-up period median (range) (months) | PFS | LCR |
|---|---|---|---|---|---|---|---|
| Mayo Clinic (30) | SRS | 88 | 10 (2.3–30) | >3 (3%) | 35 (12–83) | 95.0% | — |
| University of Pittsburgh (24) | SRS | 60 | 13.7[a] (0.8–56.8) | >13 (21%) | 35[a] (12–101) | — | 86.7% |
| University of Pittsburgh (10) | SRS | 155 | 6.5 (0.5–52.4) | Unknown | 39[a] (2–145) | — | 93.1% |
| University Hospital, Verona (25) | SRS | 111 | 8.1[a] (1–20) | 0 (0%) | 48.2 (12.1–82.5) | 96.0% | 97.0% |
| CHU La Timone (4) | SRS | 32 | 2.28[a] (0.25–60) | 2 (6%) | 56[a] (24–118) | 100.0% | — |
| University of Pittsburgh (26) | SRS | 219 | 5.0 (0.47–56.5) | 0 (0%) | 29 (2–164) | — | 93% |
| Medical University Graz (28) | SRS | 200 | 6.5 (0.38–89.8) | Unknown | 94.8 (60–144) | 98.5% | — |
| Seoul National University (11) | SRS | 63 | 6.3[a] (0.5–18.4) | 1 (2%) | 77[a] (48–112) | 90.2% | — |
| University of Pittsburgh (29) | SRS | 168 | 6.1 (0.3–32.5) | 35 (21%) | 72 (–254) | 91.0% | 97% (at 10 years) |
| University of California (27) | FSRT | 45 | 14.5 (1.4–65.66) | 8 (31%) | 36 (12–53) | 97.4% (3 years) | — |
| Hokkaido University (9.1 cc>) | FSRT | 14 | 4.7 (1.1–9.0) | 4 (28.6%) | 79.0 (27–154) | 100.0% | 100.0% |
| Hokkaido University (all cases) | FSRT | 27 | 9.1 (1.1–86.1) | 12 (44.4%) | 63.0 (19–154) | 84.6% | 88.6% |

SRS, stereotactic radiosurgery.
[a]Mean.

and FSRT (30,31). Elia et al. (30) summarized that FSRT has toxicity equivalent to that of SRS, despite its biased use for larger meningiomas with more complicated volumes. Minniti et al. (31) recommended SRS only for tumors <3 cm away more than 3 mm from the optic pathway because of the high risk of long-term neurological deficits.

Selch et al. (27) reported an encouraging 3-year PFS of 97% after FSRT for patients with a median tumor volume of 14.5 cc using a dose fractionation schedule similar to that in our study. Milker-Zabel et al. (5) have published results of FSRT for 179 skull base meningiomas, achieving 90.5 and 89% recurrence-free survival rates for benign meningiomas and atypical meningiomas, respectively, and using a median dose of 57.6 Gy (range: 45–68 Gy). Their results were excellent considering that the median target volume was as large as 33.6 $cm^3$ (1–412.6 $cm^3$) and as many as 141 (44.5%) cases of recurrent disease were included. Eight (4.4%) patients developed new clinical symptoms, such as reduced vision, trigeminal neuralgia and intermittent tinnitus located at the side of the irradiated meningioma after FSRT in their series. The slightly higher dose used in their study might have been the reason for the better tumor control with a little higher complication rate compared with our study. Korah et al. (6) used FSRT, 3D-CRT and SRS for 9, 11 and 22 patients, respectively, and among these, only 1 patient treated with SRS developed a symptomatic radiation-related neurological complication. There were no late adverse reactions in our series (27). Considering that a lower complication rate is an extremely important issue for patients with benign tumors, FSRT is one of the initial treatment options for patients with intracranial skull base meningioma which locate very close to the critical portion of normal brain tissues.

However, in our relapse cases, the LCR was low. We consider that the 2–3 mm PTV margin was sufficient with our FSRT technique by adding MLC margin to cover the PTV with 90–95% isodose line. However, it is not deniable that the high relapse rate of the larger tumors may also be explained by the small PTV margins used in our study. Goldsmith et al. (32) reported that the PFS rate in the group treated with a minimum tumor dose of >52 Gy was better than the group treated with ≤52 Gy (93 vs. 65%; $P = 0.04$). When FSRT was used for treating the case of the tumor located near the organ at risk (OAR), we must have reduced the margin for PTV to exclude the OAR from the high-dose area. Thus, the dose concentration for the tumor was gotten worse than an ideal dose distribution. Intensity-modulated radiotherapy (IMRT) is expected to increase the therapeutic ratio by reducing the dose to normal tissue because IMRT can deliver the prescription dose to the targets without worsen the dose concentration. For improvement of the LCR of those relapse cases, IMRT with a fractionated schedule will be more appropriate than simple FSRT to increase the dose for these tumors without increasing the dose to the surrounding normal tissue (33–36). However, higher radiation dose to the rest of the body and higher cost to the patient must be taken into account for each patient to use IMRT.

In conclusion, the long-term outcome suggests that FSRT is a safe and effective treatment for intracranial skull base benign meningioma, especially for those who have tumors <9.1 cc or would receive FSRT with or without surgery as the initial treatment.

## Funding

This study was partly supported by Grant-in-Aid for Scientific Research (no. 21249065) from Ministry of Education, Culture, Sports, Science and Technology, Japan, and a part of this study was presented in the poster session of 51th Annual Meeting of ASTRO in Chicago (USA), 1–5 November 2009.

## Conflict of interest statement

None declared.

## References

1. Condra KS, Buatti JM, Mendenhall WM, Friedman WA, Marcus RB, Jr, Rhoton AL. Benign meningiomas: primary treatment selection affects survival. *Int J Radiat Oncol Biol Phys* 1997;39:427–36.
2. Whittle IR, Smith C, Navoo P, Collie D. Meningiomas. *Lancet* 2004;363:1535–43.
3. Kondziolka D, Flickinger JC, Perez B. Judicious resection and/or radiosurgery for parasagittal meningiomas: outcomes from a multicenter review. Gamma Knife Meningioma Study Group. *Neurosurgery* 1998;43:405–13; discussion 13–4.
4. Roche PH, Pellet W, Fuentes S, Thomassin JM, Regis J. Gamma knife radiosurgical management of petroclival meningiomas results and indications. *Acta Neurochir (Wien)* 2003;145:883–8; discussion 8.
5. Milker-Zabel S, Zabel A, Schulz-Ertner D, Schlegel W, Wannenmacher M, Debus J. Fractionated stereotactic radiotherapy in patients with benign or atypical intracranial meningioma: long-term experience and prognostic factors. *Int J Radiat Oncol Biol Phys* 2005;61:809–16.
6. Korah MP, Nowlan AW, Johnstone PA, Crocker IR. Radiation therapy alone for imaging-defined meningiomas. *Int J Radiat Oncol Biol Phys* 2010;76:181–6.
7. Milker-Zabel S, Zabel-du Bois A, Huber P, Schlegel W, Debus J. Fractionated stereotactic radiation therapy in the management of benign cavernous sinus meningiomas : long-term experience and review of the literature. *Strahlenther Onkol* 2006;182:635–40.
8. Litre CF, Colin P, Noudel R, Peruzzi P, Bazin A, Sherpereel B, et al. Fractionated stereotactic radiotherapy treatment of cavernous sinus meningiomas: a study of 100 cases. *Int J Radiat Oncol Biol Phys* 2009;74:1012–7.
9. Simpson D. The recurrence of intracranial meningiomas after surgical treatment. *J Neurol Neurosurg Psychiatry* 1957;20:22–39.
10. Lee JY, Niranjan A, McInerney J, Kondziolka D, Flickinger JC, Lunsford LD. Stereotactic radiosurgery providing long-term tumor control of cavernous sinus meningiomas. *J Neurosurg* 2002;97:65–72.
11. Han JH, Kim DG, Chung HT, Park CK, Paek SH, Kim CY, et al. Gamma knife radiosurgery for skull base meningiomas: long-term radiologic and clinical outcome. *Int J Radiat Oncol Biol Phys* 2008;72:1324–32.
12. De Jesus O, Sekhar LN, Parikh HK, Wright DC, Wagner DP. Long-term follow-up of patients with meningiomas involving the cavernous sinus: recurrence, progression, and quality of life. *Neurosurgery* 1996;39:915–9; discussion 9–20.
13. Mathiesen T, Lindquist C, Kihlstrom L, Karlsson B. Recurrence of cranial base meningiomas. *Neurosurgery* 1996;39:2–7; discussion 8–9.
14. Maroon JC, Kennerdell JS, Vidovich DV, Abla A, Sternau L. Recurrent spheno-orbital meningioma. *J Neurosurg* 1994;80:202–8.
15. Black PM, Villavicencio AT, Rhouddou C, Loeffler JS. Aggressive surgery and focal radiation in the management of meningiomas of the skull base: preservation of function with maintenance of local control. *Acta Neurochir (Wien)* 2001;143:555–62.
16. Debus J, Wuendrich M, Pirzkall A, Hoess A, Schlegel W, Zuna I, et al. High efficacy of fractionated stereotactic radiotherapy of large base-of-skull meningiomas: long-term results. *J Clin Oncol* 2001;19:3547–53.
17. Mendenhall WM, Morris CG, Amdur RJ, Foote KD, Friedman WA. Radiotherapy alone or after subtotal resection for benign skull base meningiomas. *Cancer* 2003;98:1473–82.
18. Al-Mefty O, Kadri P, Pravdenkova S, Sawyer JR, Stangeby C, Husain M. Malignant progression in meningioma: documentation of a series and analysis of cytogenetic findings. *J Neurosurg* 2004;101:210–8.
19. Aghi MK, Carter BS, Cosgrove GR, Ojemann RG, Amin-Hanjani S, Martuza RL, et al. Long-term recurrence rates of atypical meningiomas after gross total resection with or without postoperative adjuvant radiation. *Neurosurgery* 2009;64:56–60.
20. Ohba S, Yoshida K, Hirose Y, Ikeda E, Kawase T. Early malignant transformation of a petroclival meningothelial meningioma. *Neurosurg Rev* 2009;32:495–9.
21. Colvett KT, Hsu DW, Su M, Lingood RM, Pardo FS. High PCNA index in meningiomas resistant to radiation therapy. *Int J Radiat Oncol Biol Phys* 1997;38:463–8.
22. Maillo A, Orfao A, Espinosa AB, Sayagues JM, Merino M, Sousa P, et al. Early recurrences in histologically benign/grade I meningiomas are associated with large tumors and coexistence of monosomy 14 and del(1p36) in the ancestral tumor cell clone. *Neuro Oncol* 2007;9:438–46.
23. Nakane Y, Natsume A, Wakabayashi T, Oi S, Ito M, Inao S, et al. Malignant transformation-related genes in meningiomas: allelic loss on 1p36 and methylation status of p73 and RASSF1A. *J Neurosurg* 2007;107:398–404.
24. Subach BR, Lunsford LD, Kondziolka D, Maitz AH, Flickinger JC. Management of petroclival meningiomas by stereotactic radiosurgery. *Neurosurgery* 1998;42:437–43; discussion 43–5.
25. Nicolato A, Foroni R, Alessandrini F, Maluta S, Bricolo A, Gerosa M. The role of Gamma Knife radiosurgery in the management of cavernous sinus meningiomas. *Int J Radiat Oncol Biol Phys* 2002;53:992–1000.
26. Flickinger JC, Kondziolka D, Maitz AH, Lunsford LD. Gamma knife radiosurgery of imaging-diagnosed intracranial meningioma. *Int J Radiat Oncol Biol Phys* 2003;56:801–6.
27. Selch MT, Ahn E, Laskari A, Lee SP, Agazaryan N, Solberg TD, et al. Stereotactic radiotherapy for treatment of cavernous sinus meningiomas. *Int J Radiat Oncol Biol Phys* 2004;59:101–11.
28. Kreil W, Luggin J, Fuchs I, Weigl V, Eustacchio S, Papaefthymiou G. Long term experience of gamma knife radiosurgery for benign skull base meningiomas. *J Neurol Neurosurg Psychiatry* 2005;76:1425–30.
29. Flannery TJ, Kano H, Lunsford LD, Sirin S, Tormenti M, Niranjan A, et al. Long-term control of petroclival meningiomas through radiosurgery. *J Neurosurg* 2010;112:957–64.
30. Elia AEH, Shih HA, Loeffler JS. Stereotactic radiation treatment for benign meningiomas. *Neurosurg Focus* 2007;23:E5.
31. Minniti G, Amichetti M, Enrici RM. Radiotherapy and radiosurgery for benign skull base meningiomas. *Radiat Oncol* 2009;4:42.
32. Goldsmith BJ, Wara WM, Wilson CB, Larson DA. Postoperative irradiation for subtotally resected meningiomas. A retrospective analysis of 140 patients treated from 1967 to 1990. *J Neurosurg* 1994;80:195–201.
33. Khoo VS, Oldham M, Adams EJ, Bedford JL, Webb S, Brada M. Comparison of intensity-modulated tomotherapy with stereotactically guided conformal radiotherapy for brain tumors. *Int J Radiat Oncol Biol Phys* 1999;45:415–25.
34. Pirzkall A, Carol M, Lohr F, Hoss A, Wannenmacher M, Debus J. Comparison of intensity-modulated radiotherapy with conventional conformal radiotherapy for complex-shaped tumors. *Int J Radiat Oncol Biol Phys* 2000;48:1371–80.
35. Pirzkall A, Debus J, Haering P, Rhein B, Grosser KH, Hoss A, et al. Intensity modulated radiotherapy (IMRT) for recurrent, residual, or untreated skull-base meningiomas: preliminary clinical experience. *Int J Radiat Oncol Biol Phys* 2003;55:362–72.
36. Milker-Zabel S, Zabel-du Bois A, Huber P, Schlegel W, Debus J. Intensity-modulated radiotherapy for complex-shaped meningioma of the skull base: long-term experience of a single institution. *Int J Radiat Oncol Biol Phys* 2007;68:858–63.

JOURNAL OF APPLIED CLINICAL MEDICAL PHYSICS, VOLUME 12, NUMBER 3, SUMMER 2011

# Detection of patient setup errors with a portal image – DRR registration software application

Kenneth Sutherland,[1a] Masayori Ishikawa,[1] Gerard Bengua,[2] Yoichi M. Ito,[1] Yoshiko Miyamoto,[1] and Hiroki Shirato[1,2]
*Hokkaido University Graduate School of Medicine,[1] Sapporo 060-8648, Japan; Hokkaido University Hospital,[2] Sapporo 060-8648, Japan*
*kensuth@med.hokudai.ac.jp*

Received 25 October, 2010; accepted 13 February, 2011

The purpose of this study was to evaluate a custom portal image — digitally reconstructed radiograph (DRR) registration software application. The software works by transforming the portal image into the coordinate space of the DRR image using three control points placed on each image by the user, and displaying the fused image. In order to test statistically that the software actually improves setup error estimation, an intra- and interobserver phantom study was performed. Portal images of anthropomorphic thoracic and pelvis phantoms with virtually placed irradiation fields at known setup errors were prepared. A group of five doctors was first asked to estimate the setup errors by examining the portal and DRR image side-by-side, not using the software. A second group of four technicians then estimated the same set of images using the registration software. These two groups of human subjects were then compared with an auto-registration feature of the software, which is based on the mutual information between the portal and DRR images. For the thoracic case, the average distance between the actual setup error and the estimated error was 4.3 ± 3.0 mm for doctors using the side-by-side method, 2.1 ± 2.4 mm for technicians using the registration method, and 0.8 ± 0.4 mm for the automatic algorithm. For the pelvis case, the average distance between the actual setup error and estimated error was 2.0 ± 0.5 mm for the doctors using the side-by-side method, 2.5 ± 0.4 mm for technicians using the registration method, and 2.0 ± 1.0 mm for the automatic algorithm. The ability of humans to estimate offset values improved statistically using our software for the chest phantom that we tested. Setup error estimation was further improved using our automatic error estimation algorithm. Estimations were not statistically different for the pelvis case. Consistency improved using the software for both the chest and pelvis phantoms. We also tested the automatic algorithm with a database of over 5,000 clinical cases from our hospital. The algorithm performed well for head and breast but performed poorly for pelvis cases, probably due to lack of contrast in the megavoltage portal image. The software incorporates an original algorithm to fuse portal and DRR images, which we describe in detail. The offset optimization algorithm used in the automatic mode of operation is also unique, and may be useful if the contrast of the portal images can be improved.

PACS numbers: 87.55.Qr, 87.57.nj

Key words: patient setup, image registration, portal imaging, mutual information

[a] Corresponding author: Kenneth Sutherland, Hokkaido University Graduate School of Medicine, Sapporo-shi Kita-ku Kita 14 Jo Nishi 5 Chome, 060-8648 Japan; phone:+81-11-706-7638; fax:+81-11-706-7639; email: kensuth@med.hokudai.ac.jp

## I. INTRODUCTION

Traditionally doctors have judged patient setup errors by viewing portal images alongside planning digital reconstructed radiograph (DRR) images, either with paper printouts, films on a light board, or on a computer terminal. Estimation of the error is made by measuring the distance from the isocenter to anatomical structures (usually bones) visible in both images.[1] However, the process is often inaccurate, with errors between 5 and 10 mm being reported.[2]

Fully and semi-automatic methods based on electronic portal imaging devices (EPIDs),[3] implanted fiducial surrogate markers imaged with kilovoltage fluoroscopy,[4] on-board imager (OBI, Varian Medical Systems, Palo Alto, CA)[5] and cone-beam CT (CBCT), have recently become common. However, these methods often require additional cost, exposure of X-rays, and longer time for setup. As a result, for a large number of patients who do not require a high accuracy of patient positioning (e.g., palliative treatments or mantle field radiation), portal imaging once or twice during the first week of treatment is still desirable.

The standard patient treatment regime employed at our institution involves first obtaining a CT scan of the patient which will be used for treatment planning. A DRR reconstruction of the beam's eye view (BEV) is computed and stored by a commercial treatment planning system (TPS). The treatment port, isocenter, orthogonal axes with scale information (a tick mark each centimeter) and other treatment information are burned into the DRR image.

Portal images are usually obtained at our hospital before the first treatment fraction using a megavoltage X-ray source from a linear accelerator and a computed radiograph (CR) system (Fuji Medical Co., Ltd., Tokyo, Japan). Images are captured onto photosensitive plates, which are scanned to produce high resolution (usually $1760 \times 1760$ pixels) deep bit (10 bits per pixel) images. The portal images also contain scale information on the orthogonal axes with a small dot each centimeter. The portal and DRR images are compared to determine that the treatment beam accurately targets the planned treatment volume (PTV) while avoiding organs at risk (OARs). If a problem is detected, the presiding physician may request that the couch position be adjusted. Portal images are then retaken and rechecked against the DRR.

We developed an image registration software application for the estimation of patient setup error. DRRs from any commercial TPS can be opened using common file formats (e.g., bitmap, JPEG, DICOM). The software works for any anatomical region or gantry angle. The software can be operated manually, or with an automatic registration mode based on the mutual information between the images.

The purpose of this study is to verify that our software actually improves setup error detection compared with the traditional side-by-side method. There is little statistical evidence in the literature of the superiority of image registration to side-by-side human estimation of setup error from two-dimensional portal images. We evaluated the efficacy of the software as an aid for the clinical staff to improve setup accuracy using a prospective phantom study and its statistical analysis. We compared the ability of humans to correctly determine a known setup error with and without the software. An automatic mode of operation of the software was also tested with a database of clinical cases, collected over several years, for which the setup up error was determined by the consensus of a trained software operator (medical physicist), a radiation technician and the presiding oncologist.

## II. MATERIALS AND METHODS

### A. Patient setup error detection software

After a CT scan of the patient is obtained, a DRR of the BEV is computed and stored with a TPS. The treatment port, isocenter, orthogonal axes with scale information (a tick mark each centimeter) and other treatment information are burned into the image. The DRR image is

saved in a database accessible to our software. Portal images are usually obtained before the first treatment fraction using a double exposure (open field and the actual field) with a megavoltage X-ray source from a linear accelerator, captured with a CR system. The portal images also contain graphical scale information on the orthogonal axes with a small dot or tick mark every centimeter from the isocenter.

In our proposed method, while the patient is lying on the treatment couch, the planning DRR and portal images are loaded into the software. The isocenter and two points on orthogonal axes, usually 10 cm from the isocenter, are designated by clicking on the images with the mouse. The locations of the points are determined by the operator using the axis and scale tick marks on each image. The software uses the three control points to determine scaling and rotation in order to transform the portal image into the coordinate space of the DRR image. Because the imaging plate may not be exactly orthogonal to the beam axis, especially when an oblique gantry angle is used, the portal image may be warped. The software can correct for these out-of-plane rotations.

After the images have been successfully fused, the operator uses bony landmarks or other visible anatomical features in order to determine setup error. The portal image can be shifted horizontally or vertically and rotated clockwise or counterclockwise relative to the stationary DRR image. An example screenshot is shown in Fig. 1.

The operator can apply complementary colors, such as red and cyan, to make the fused image more distinguishable. If the images align exactly, each resulting pixel will be a level of grey. Misalignments are visible as color shadows. The operator can specify which pair of complementary colors to apply, depending on which colors are easier to see. Brightness and contrast can also be adjusted on both images to make bony features more distinguishable. The user can also rapidly flip between the DRR, portal and fused images. After the images are successfully registered, the treatment field shift (in mm) and rotation (in degrees), corresponding to the BEV, is displayed. The required couch movement to correct the offset, based on the gantry angle, can also be computed and displayed.

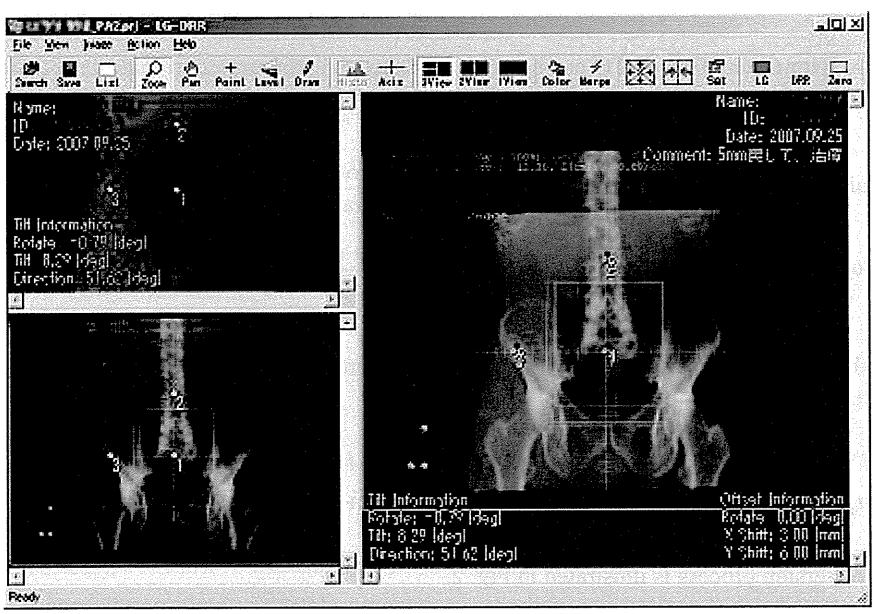


FIG. 1. The Portal-DRR software. The user specifies three points on the portal (top left) and DRR (bottom left) images using grid spacing tick marks.The merged image (right) is used to compare internal bony structures in order to determine the setup error, which is displayed at the lower right.

## B. Theory of image distortion correction

Distortions of portal images may include rotations about the beam axis (z-axis) and rotations about an axis perpendicular to the beam axis (x- or y-axis). It is difficult to independently correct rotations about the x and y axes. We therefore devised a scheme to treat rotations about the x and y axes as equivalent rotations about an arbitrary axis perpendicular to the z-axis, denoted as the x'-axis. The x'-axis lies in the x, y plane and points in the direction of the tilt. It is possible to compose rotations about the x'-axis from equivalent rotations about the x and y axes, combined with a rotation about the z-axis. Coordinates on the imaging plate (x', y') correspond to the original coordinates (x, y) as follows:

$$\begin{pmatrix} x' \\ y' \end{pmatrix} = b \cdot Rot(\theta) \cdot Rot(\varphi) \cdot St(\phi) \cdot Rot^{-1}(\varphi) \begin{pmatrix} x \\ y \end{pmatrix} \tag{1}$$

Here $b$ is the zoom ratio, $Rot(\theta)$ is the rotation about the z-axis, Rot($\phi$) is the rotation about the x'-axis, and St($\Theta$) is the stretch ratio produced by the rotation about the x-axis. The rotation and stretch functions are defined as:

$$\text{Rot}(\theta) = \begin{pmatrix} \cos\theta & -\sin\theta \\ \sin\theta & \cos\theta \end{pmatrix}, St(\phi) = \begin{pmatrix} 1 & 0 \\ 0 & \dfrac{1}{\cos\phi} \end{pmatrix} \tag{2}$$

One can obtain the original image pixel coordinates by applying the reverse process in order to correct the distorted image:

$$\begin{pmatrix} x \\ y \end{pmatrix} = \frac{1}{b} \cdot Rot(\varphi) \cdot St^{-1}(\phi) \cdot Rot^{-1}(\varphi) \cdot Rot^{-1}(\theta) \begin{pmatrix} x' \\ y' \end{pmatrix} \tag{3}$$

Because parameters $\theta$, $\phi$, and $\Theta$ can be obtained from two arbitrary coordinates, according to the equations, we can proceed as follows.

$$\begin{aligned} \varphi &= \arctan\left(\frac{1}{2}\left(\alpha + \sqrt{4+\alpha^2}\right)\right) \qquad \varphi + \theta = arctan\left(\frac{m\cos\varphi + n\sin\varphi}{k\cos\varphi + l\sin\varphi}\right) \\ \phi &= \cos^{-1}\left(\frac{m\cos\varphi + n\sin\varphi}{k\sin\varphi - l\cos\varphi}\right) \qquad b = \frac{\cos(\varphi+\theta)}{k\cos\varphi + l\sin\varphi} \end{aligned} \tag{4}$$

Note that k, l, m and n are in the original beam axis' coordinate system and can be computed from two pairs of points.

$$\begin{pmatrix} k & l \\ m & n \end{pmatrix} = \begin{pmatrix} x_1 & x_2 \\ y_1 & y_2 \end{pmatrix} \begin{pmatrix} x'_1 & x'_2 \\ y'_1 & y'_2 \end{pmatrix}^{-1} = \frac{1}{x'_1 y'_2 - x'_2 y'_1} \cdot \begin{pmatrix} x_1x'_1 + x_2y'_1 & x_1x'_2 + x_2y'_2 \\ y_1x'_1 + y_2y'_1 & y_1x'_2 + y_2y'_2 \end{pmatrix} \tag{5}$$

The conversion process is illustrated in Fig. 2.

The proposed image-registration method uses imaging plates to obtain portal images for irradiation field verification. For non-zero gantry angles, the imaging plate is held freely on a stand without fixation to a certain coordinate system. In order to correct perspective distortion due to the imaging plate not being orthogonal to the beam axis, three control points are

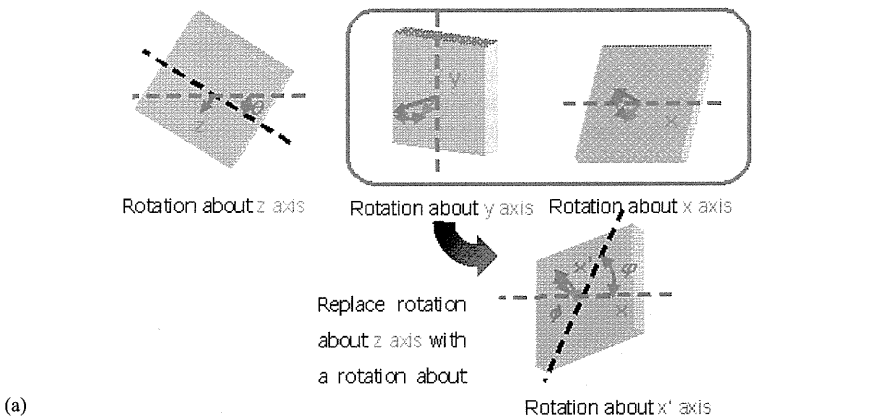


(a)

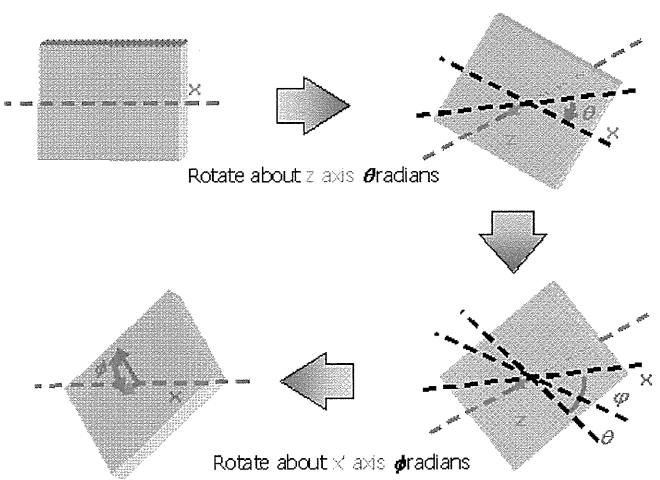


(b)

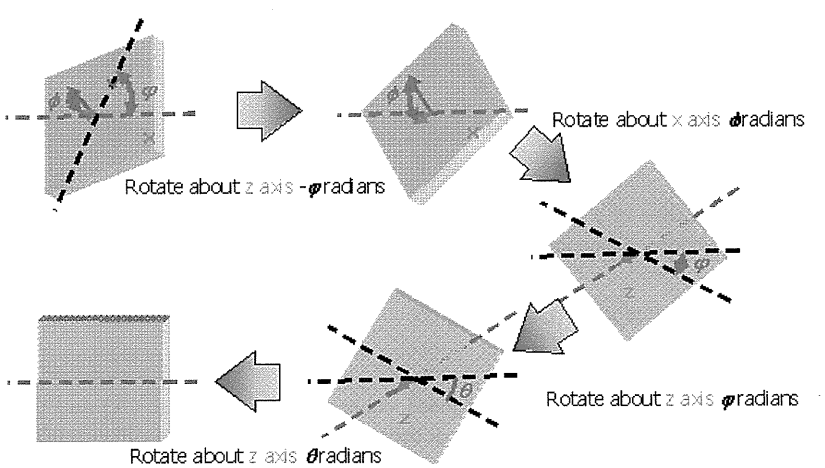


(c)

FIG. 2. Conversion of rotation axis for image distortion.

manually placed using graphical axis scale tick marks on each image. The specified points should cover the area of the image containing bony structures used for alignment. We refer to the area roughly surrounding the control points as the "working area".

To test the correction function, an electronic tiltmeter was used to measure a 10° tilt of the imaging plate about the horizontal axis. The plate was exposed to X-rays using the linac axis grid. The resulting image was fused with a dummy DRR image. A test point was placed at a position 5 cm along the x- and y-axis within the working area. The distance from the test point on the DRR image and the transformed portal image point was measured. The experiment was repeated with the test point outside the working area. The experimental setup is illustrated in Fig. 3.

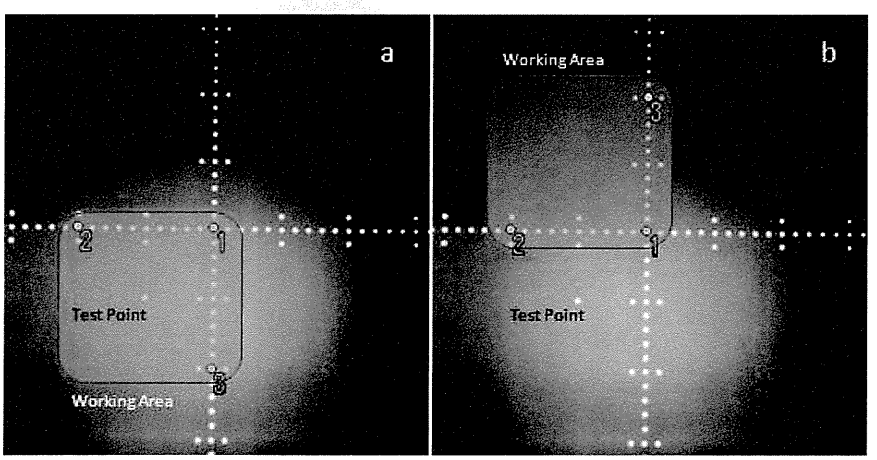


FIG. 3. Tilt experiment setup. The imaging plate was tilted 10° horizontally. The test point (5 cm along the x- and y-axis) was inside the working area for (a) and outside the working area for (b). The test point was transformed into the DRR image coordinates and the distance from the corresponding point specified on the DRR image was measured.

### C. Automatic determination of patient setup error

We developed a method to automatically determine the x-y shift and in-plane rotation based on the mutual information (MI) of the pixel intensity values of the overlapping portions of the transformed portal and DRR images. The entropy of a single image can be computed from the equation:

$$H = \sum_i p_i \cdot \log \frac{1}{p_i} \tag{6}$$

where $p_i$ is the probability of a gray-level pixel value $i$ estimated from the histogram of the image.[6] The joint entropy between two images can likewise be defined as:

$$H(A,B) = -\sum_{i,j} p(i,j) \cdot \log[p(i,j)] \tag{7}$$

where $p(ij)$ is the probability of gray-level pixel value $i$ from one image (A) and the gray-level pixel value $j$ from the second image (B) at the same position. Mutual information is then defined as:

$$I(A,B) = H(A) + H(B) - H(A,B) \tag{8}$$

where *H(A)* is the entropy of the first image (i.e., the portal image), *H(B)* is the entropy of the second image (i.e., the DRR image), and *H(A,B)* is the entropy of their joined histogram.[7]

Optimizing the MI involves finding the x-y shift position that yields the highest mutual information coefficient, automatically shifting the portal image left, right, up and down a determined step size, and choosing the position with the highest MI coefficient. If the current x-y shift value yields the highest MI coefficient, the optimization loop is abandoned. In order to reduce the likelihood of stopping at a local maximum, we employ a multiresolution method. The initial step size is relatively large, usually 4 mm. The best MI coefficient is located with the initial step size. The step size is then reduced by half and the process is repeated. The final step size is usually 1 mm, but can be set lower for submillimeter accuracy.

Adding rotation checks can increase optimization time exponentially if every possible rotation is checked at each shift location. However, if we assume that the setup rotation is small, a good compromise approach is to search rotation and shift iteratively; that is, search for the best x-y shift and then search for the best rotation. This process is repeated until the best possible rotation is found at the best possible x-y shift.

## D. Phantom study

CT scans of anthropomorphic thorax and pelvis phantoms were taken. The images were read into a commercial treatment planning software system (Xio; CMS, Inc., St. Louis, MO). DRR images (one for the thorax, one for the pelvis) were generated using an antero-posterior (AP) port with a $10 \times 10$ cm square field.

In order to be able to present a portal image with a known but arbitrary x-y error offset, we first obtained a single portal image of the phantom without field or scale ticks. Our test software burns in the treatment field and tick marks based on determined horizontal and vertical offset error values (Fig. 4). The portal images of the phantoms were acquired with a 6 MV photon beam from a linear accelerator. A list of five cases was prepared with offset values between plus and minus 10 mm horizontally and vertically. Rotation was not considered in this study. In order to determine each subject's consistency in determining the offset error, each case was presented twice for a total of ten cases. Each subject was presented with the same offset cases, but the order of the case list was shuffled.

For the ten thorax and ten pelvis cases generated by the computer with the above method, we presented the series of cases to each examiner using three methods. First, five licensed radiation oncologists determined setup error with the conventional side-by-side method, without the aid of the registration software. We refer to this as the "side-by-side method". These doctors included experienced physicians, as well as doctors in training. Four radiation technicians were

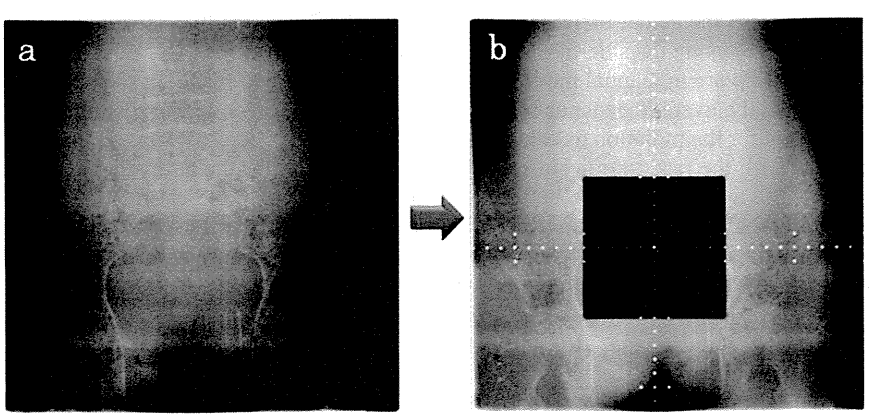


FIG.. 4. Portal image taken without field or scale tick marks (a). Automatically generated treatment field and scale ticks applied to the phantom portal image (b).

then asked to determine the same series of setup errors using the registration software, which we refer to as the "registration method". The automatic determination function of the software was also used to determine the setup error of the same case list ("automatic method"). Doctors and technicians were allowed to adjust image brightness and contrast. No time constraint was in place during the testing.

### E. Statistical analysis

The distance from actual and estimated offset was computed with $\sqrt{(x-x_0)^2+(y-y_0)^2}$ where (x, y) is the estimated offset and ($x_0$, $y_0$) is the actual offset. The average and standard deviation of the distance was computed for each examiner.

The average consistency of an examiner was defined as the average geometric distance between two estimations of a single case. The mean of the methods was compared with the paired t-test. The difference of the average consistency among the three methods was also computed in order to determine if consistency improved using the software. All statistical analysis was performed with JMP version 8 (SAS Institute Inc., Cary, NC).

### F. Database study

In order to test the performance of the automatic registration mode of the software on actual clinical data, we assembled a database of over 5,000 patient setup cases performed between April 2007 and December 2009 at our hospital. At the time of treatment, the portal image for each case was registered with the corresponding DRR image using the manual mode of the software, and the setup error for each case was determined by a consensus of three people: a software operator (medical physicist), a radiation technician, and the attending oncologist. Although it is difficult to establish a "gold standard" for clinical data, for this study we assume the human-determined offset is correct, or at least very near the actual offset error.

After assembling the database, a large batch script was executed to open each case, fuse the portal and DRR images, and automatically determine the error offset using the MI optimization algorithm described above. The automatically-determined error offset was then compared with the human-determined error offset. The geometric distance between the two values was computed and a statistical analysis was performed.

## III. RESULTS

### A. Phantom study

The results of the thoracic and pelvis are shown in Fig. 5(a) and 5(b), respectively. The geometric distance from the actual offset and the determined offset is plotted. Results from five doctors (DR1–DR5) using the side-by-side method, four technicians (TECH1–TECH4) using the registration software in manual mode, and the automatic method (COMP) are shown.

For the thorax, the average distance between the actual setup error and the estimated error was 4.3 ± 3.0 mm for the radiation oncologists without the registration software, 2.1 ± 2.4 mm for technicians with the registration software, and 0.8 ± 0.4 mm for the automatic algorithm. For the pelvis, the average distance between the actual setup error and estimated error was 2.0 ± 0.5 mm for the radiation oncologists without the registration software, 2.5 ± 0.4 mm for technicians with the registration software, and 2.0 ± 1.0 mm for the automatic algorithm.

Each case was presented to the examiner twice. These two values are plotted vertically for each examiner. Consistency was measured as the geometric distance between the two estimated offsets of the same portal image. This corresponds to the height of the vertical bar in Fig. 5. The results are summarized in Table 1.

In order to determine statistically whether setup error estimation improved using the software, we computed the average consistency among the three methods. The average consistency for the side-by-side method was 2.4 ± 2.0 mm for thorax and 1.4 ± 1.2 mm for pelvis. The average

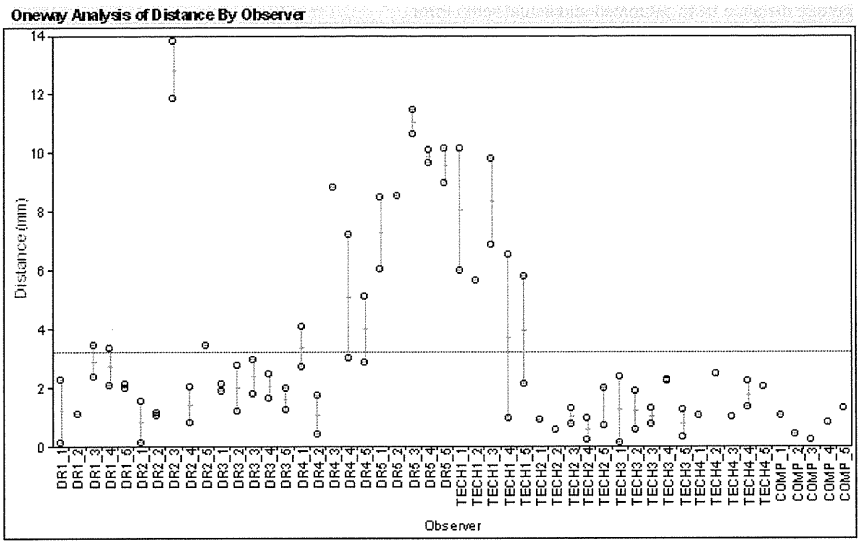


(a)

FIG. 5(a). Results of AP chest study.

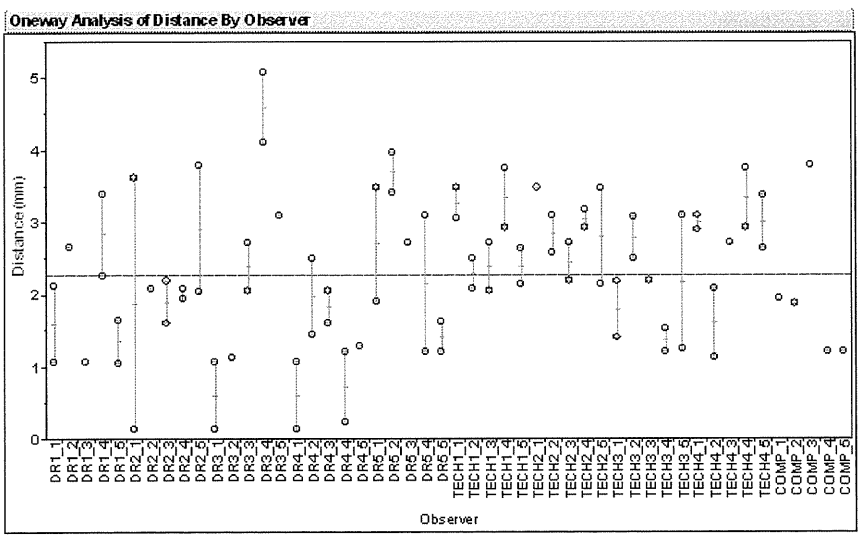


(b)

FIG. 5(b). Results of AP pelvis study.

consistency for the registration method was $1.7 \pm 1.6$ mm for thorax and $0.9 \pm 0.5$ mm for pelvis. The results are summarized in Table 2. Note that the computer algorithm always produces the same result for a given input, so it is perfectly consistent.

In order to test statistically that setup error estimation improved using the software, we computed the paired two samples for means. The null hypothesis is that population mean of the differences between the paired values is zero. The results are summarized in Tables 3(a) and 3(b).

TABLE 1. Average distance from estimated and actual setup error.

| *Phantom* | *Method* | *Average Distance* |
|---|---|---|
| Chest | Side-by-side | 4.3±3.0 mm |
| | Registration | 2.1±2.4 mm |
| | Auto | 0.8±0.4 mm |
| Pelvis | Side-by-side | 2.0±0.5 mm |
| | Registration | 2.5±0.4 mm |
| | Auto | 2.0±1.0 mm |

TABLE 2. Average consistency of test subjects.

| *Phantom* | *Method* | *Average Consistency* |
|---|---|---|
| Chest | Side-by-side | 2.4±2.0 mm |
| | Registration | 1.7±1.6 mm |
| Pelvis | Side-by-side | 1.4±1.2 mm |
| | Registration | 0.9±0.5 mm |

TABLE 3(a). Comparison of estimation methods (chest).

| *Comparison* | *p-value* |
|---|---|
| Side-by-side - Registration | 0.0067 |
| Side-by-side - Auto | 0.0002 |
| Registration - Auto | 0.0001 |

TABLE 3b. Comparison of estimation methods (pelvis).

| *Comparison* | *p-value* |
|---|---|
| Side-by-side - Registration | 0.0047 |
| Side-by-side - Auto | 0.4547 |
| Registration - Auto | 0.0593 |

## B. Database study

Results of the database study are summarized in Table 4. Overall, the automatic registration method does not perform well at around 7 mm from the human-estimated offset. However, for certain anatomical regions, such as head and breast, the algorithm consistently estimated the setup error within about 2 mm of the human estimation. Automatic registration was especially poor for pelvic regions — more than 1 cm on average. This is probably due to the lack of contrast in the portal images.

In order to demonstrate the usefulness of the automatic mode of operation for two sample anatomical cases, we arbitrarily divided the distance between the human and computer estimated offsets into four bins: ≤ 2 mm (Good), ≤ 5 mm (Fair), ≤ 10 mm (Poor) and > 10 mm (Terrible). Tables 5(a) and 5(b) show the results for head and pelvis cases for all gantry angles.

TABLE 4. Comparison of auto-shift function with clinical case database.

| *Group* | *Count* | *Mean Dist. (mm)* |
|---|---|---|
| All | 5101 | 7.0±2.1 |
| AP Head | 407 | 2.4±2.1 |
| LR Head | 537 | 2.2±2.7 |
| AP Neck | 158 | 5.5±6.1 |
| LR Neck | 214 | 4.2±4.3 |
| OB Neck | 95 | 4.8±4.1 |
| AP Chest | 264 | 5.1±4.5 |
| LR Chest | 101 | 7.7±8.0 |
| OB Breast | 160 | 3.6±2.7 |
| AP Pelvis | 148 | 13.8±19.8 |
| LR Pelvis | 148 | 12.8±11.7 |

TABLE 5(a). Comparison of auto-shift function with humans (head).

| *Bin* | *Frequency (total = 61)* |
|---|---|
| Good (≤2 mm) | 35 (57%) |
| Fair (≤5 mm) | 23 (38%) |
| Poor (≤10 mm) | 1 (2%) |
| Terrible (> 10 mm) | 2 (3%) |

TABLE 5(b). Comparison of auto-shift function with humans (pelvis).

| *Bin* | *Frequency (total = 48)* |
|---|---|
| Good (≤2 mm) | 4 (8%) |
| Fair (≤5 mm) | 9 (19%) |
| Poor (≤10 mm) | 16 (33%) |
| Terrible (> 10 mm) | 19 (40%) |

### C. Tilt experiment

Results of the tilt experiment are presented in Table 6. When the test point was placed 5 cm within the working area, the distance from the DRR point and the transformed portal image point was 0.7 mm. When the point was placed 5 cm outside the working area, the distance increased to 1.5 mm. This result indicates that the user must be careful to consider only bony structures within the working area when the out-of-plane tilt is large. The automatic registration algorithm should also ignore pixels outside the working area.

TABLE 6. Result of tilt experiment.

| *Point Placement* | *Distance* |
|---|---|
| Inside working area | 0.7 mm |
| Outside working area | 1.5 mm |

## IV. DISCUSSION

Our results show that the registration method was at least not worse than the side-by-side method, and the automatic method was statistically better than both the side-by-side method and registration method for the thorax phantom case studied. This result suggests that our

software can be a reasonable complementary method in the clinical practice. Based on this study, the software has been installed in our hospital information system and has been used in clinical practice since April 2007. Moreover, the time required for the estimation of the setup error has not been extended by the usage of this program, once the operator obtained sufficient experience with the software.

A number of criteria influenced our software design decisions:

- Because image registration is performed while the patient is waiting in the treatment position, the system must be fast — less than about one minute after the portal image is obtained.
- DRRs by any commercial planning software are to be used, as long as scale information is burned into the bitmap. The DRR image can even be a screen-captured bitmap, or a digital scan of a paper, or film print.
- Any common file format (e.g., bitmap, JPEG, DICOM) can be used for either the portal or DRR image.
- The system must work with any beam view of any anatomical region encountered in clinical practice.
- The software must run on a single standard PC running the Windows operating system.

We have found that there was a large inconsistency in the side-by-side method among doctors. This is probably due to a difference in training or experience. The large variation in the accuracy of the final decision based on the portal film may influence the clinical outcome. The improvement in the consistency with automatic registration (which was found in this study for thorax) may improve the local control rate and complication rate in this context.

If Dr. 5, in particular, is omitted, the side-by-side method compares well with the registration methods. Although Dr. 5 was a licensed radiation oncologist with experience estimating setup errors, he or she may have needed more practice with our experimental setup. Although we explained that the movement of the radiation field (rather than the treatment couch) should be specified, it is easy to mistake left-right or up-down shift. We feel that these kinds of human errors are inevitable when relying solely on human judgment with the side-by-side method.

From the database study, we can state that the automatic mode of operation performs well for head, neck and breast cases, but performs poorly for pelvic cases. Due to the thickness of the human anatomy in the pelvic and abdomen regions, the contrast of the resulting megavoltage portal image is very low. This makes automatic registration based on mutual information extremely difficult. In order to improve the performance of the automatic registration, the contrast of the portal image needs to be improved. Possible methods of improving portal image contrast include using kilovoltage X-ray, or using advanced digital image processing.[8] Other methods, such as restricting the area used to compute the mutual information may further improve auto-registration.

Although the automatic registration algorithm performed reasonably well on the pelvis phantom, the brightness and contrast (window level) of the portal image from the phantom image was adjusted by hand to maximize the contrast of the pelvic bone. In the database study, however, it was not feasible to adjust all cases by hand. The window level was computed automatically from the raw scanned data based on the histogram of pixel values. If the window level algorithm can be improved, the image contrast may be increased. Sophisticated image filters may also improve the signal-to-noise ratio and make bony features more recognizable.[9] We hope that this will, in turn, improve the auto-registration results.

While some verification systems are applicable to only a particular application (for example, lung cancer[10] or pelvic treatments[11]), our system is used for all cases encountered in our practice, including oblique views. Some systems require the computation of custom DRR images in order to match as closely as possible the portal image.[12] Our system uses the DRRs that are generated by a commercial TPS software package. Thus, the same pair of portal and DRR images that the attending physicians have normally been using are used by our software.